ACS OMEGA

http://pubs.acs.org/journal/acsodf

Article

Synthesis of Prussian Blue Analogue and Its Catalytic Activity toward Reduction of Environmentally Toxic Nitroaromatic Pollutants

Dina A. El Mously, Amr M. Mahmoud,* Ahmed M. Abdel-Raoof,* and Elsayed Elgazzar

Cite This: *ACS Omega* 2022, 7, 43139−43146

Read Online

ACCESS | Metrics & More | Article Recommendations | Supporting Information

ABSTRACT: Nitroanilines are environmentally toxic pollutants which are released into aquatic systems due to uncontrolled industrialization. Therefore, it is crucial to convert these hazardous nitroanilines into a harmless or beneficial counterpart. In this context, we present the chemical reduction of 4-nitroaniline (4-NA) by $NaBH_4$ utilizing Prussian blue analogue (PBA) as nanocatalyst. PBAs can serve as inexpensive, eco-friendly, and easily fabricated nanocatalysts. PBA cobalt tetracyanonickelate hexacyanochromate (CoTCNi/HCCr) was stoichiometrically prepared by a facile chemical coprecipitation. Chemical, phase, composition, and molecular interactions were investigated by XRD, EDX, XPS, and Raman spectroscopy. Additionally, SEM and TEM micrographs were utilized to visualize the microstructure of the nanomaterial. The findings revealed the synthesized PBA of the cubic phase and their particles in nanosheets. The band gap was estimated from the optical absorption within the UV−vis region to be 3.70 and 4.05 eV. The catalytic performance of PBA for the reduction of 4-NA was monitored by UV−vis spectroscopy. The total reduction time of 4-NA by PBA was achieved within 270 s, and the computed rate constant (k) was 0.0103 s^{-1}. The synthesized PBA nanoparticles have the potential to be used as efficient nanocatalysts for the reduction of different hazardous nitroaromatics.

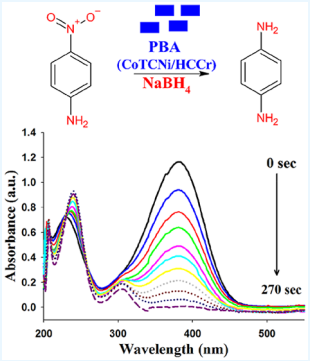

1. INTRODUCTION

Environmentally hazardous pollutants, particularly pigments and dyes, are produced from various industries such as cosmetics, textile, leather, and food processing.[1,2] Nitroaromatic compounds are environmental contaminants that are spread into the wastewater environment by numerous textile industries. Nitroanilines represent a significant class of environmentally harmful hazardous compounds.[3] They are typically carcinogenic substances that can harm human lung tissues and cause cancer.[4] Continuous efforts are exerted to either remove these hazardous compounds from the environment or alternatively break down these hazardous compounds into harmless chemicals. The breakdown of nitroanilines from environmental wastewater has been demonstrated utilizing different strategies, including microbial degradation,[5] catalytic reduction,[6] photocatalytic degradation,[7] and adsorption.[8]

The reduction of nitroaromatics to aminoaromatics is a crucial step in eliminating them and maximizing the benefits. These amino derivatives are essential intermediates in the synthesis of polymers, dyes, surfactants, and pharmaceutical products. Numerous techniques, including electrolytic reduction,[9] photoreduction,[10,11] homogeneous catalysis,[12] heterogeneous catalytic hydrogenation[13] and the use of reducing agents like hydrazine hydrates,[14] are available for reducing nitroaromatics to the respective aminoaromatics. However, these procedures have one or more drawbacks, such as low efficacy (microbial degradation), overpriced photosetups (photocatalysis), and harmful effects of the utilized chemicals. However, it was found that reduction utilizing $NaBH_4$ could be initiated in the presence of appropriate catalysts by releasing the corresponding hydride.[15] This technique is characterized by its simplicity, effective conversion rates, absence of sludge, energy, and time savings. It does not require an energy source, expensive working setups, or convenient selection of potential window as in the electrochemical removal. Therefore, it is desirable to synthesize a low-cost, highly stable catalyst for the reduction of nitroaromatic chemicals.

Various nanoparticles have been synthesized that exhibit interesting behavior such as conductive[16,17] and catalytic and optical characteristics dependent on size and surface modifications. From this perspective, the use of nanocatalysts in the reduction of nitroaromatics has received a lot of attention in the last years. They catalyze the reaction by offering a significantly greater surface area for the transfer of the electrons compared to ordinary powdered catalysts.

Many nanocatalysts have been reported in the literature for catalytic reduction of nitroarenes including Au NPs[18,19] and Ag

Received: September 2, 2022
Accepted: November 3, 2022
Published: November 16, 2022

NPs catalysts.[20,21] Although they exhibit efficient catalytic activity, however, the need for more affordable and simple nanocatalysts has driven more research in this field.

Prussian blue (PB) and its analogs metal hexacyanometallates have gained wide attention from many research groups owing to their exceptional chemical and electronic properties as well as their outstanding applications. Prussian blue analogues (PBAs) are widely utilized in fuel cells, supercapacitors, medicine, and energy storage systems depending on their small particle size, redox chemistry, high charge transfer, flexible molecular structure, and photomagnetic characteristics. Owing to their high electronegativity and spectroscopic features, the cyanide group (CN^-) can combine with the transition-metal results in producing large diversity complexes with a great variety of coordination modes.[22−24] Moreover, PB exhibits a special structure anchored to the extended porosity and transfer of charge carriers from cyanide bridge CN through nitrogen or carbon atom to a metal center creating 1D, 2D, and 3D nanomaterials with open frameworks.[23,25] Despite the aforementioned advantages, the PBAs have some drawbacks such as low conductivity and molecular aggregation. To optimize their performance and avoid these problems, conductive nanoparticles including carbon nanotubes (CNTs) or graphene could be combined with the PB framework.[26,27] Moreover, a change in the transition metal that linked nitrogen molecules to manganese (Mn), zinc (Zn), iridium (Ir), ruthenium (Ru), cadmium (Cd), copper (Cu), cobalt (Co), chromium (Cr), and palladium (Pd) creates novel complexes with excellent structural, optical, magnetic, and electrical properties.[26−28]

In this work, the PBA cobalt tetracyanonickelate hexacyanochromate (CoTCNi/HCCr) nanoparticle has been synthesized to be used as nanocatalyst for catalytic reduction of 4-nitroaniline. This modification potentially enhances the catalytic activity and performance in the reduction process of nitroaniline.

2. EXPERIMENTAL SECTION

2.1. Chemicals and Reagents. Sodium borohydride 98% purity, 4-nitroaniline ≥99% purity, potassium tetracyanonickelate (II) [$K_2Ni(CN)_4$] >99.9% purity, cobalt chloride hexahydrate 98% purity, and potassium hexacyanochromate (III) [$K_3Cr(CN)_6$] 99.99% purity were purchased from Sigma-Aldrich (Germany). Ultrapure water was obtained from "Aquatron" Automatic Water Still A4000, Bibby Sterillin Ltd., (Staffordshire, UK).

2.2. Preparation of PBA CoTCNi/HCCr. Separately, 0.6 mol of potassium tetracyanonickelate and 0.2 mol of potassium hexacyanochromate were dissolved in 20 mL of double-distilled water for 2 h using a magnetic stirrer. After that, the metal cyanide salts were added together while continuously stirring at room temperature for another 2 h. Cobalt chloride hexahydrate (0.9 mol) was dissolved into double-distilled water and then added dropwise to the mixture of metal cyanide salts with continuous stirring for 3 h until a homogeneous precipitate powder was formed. The obtained precipitate was filtered with filter paper,d washed several times with double-distilled water to remove the salt ions, subsequently dried at 70 °C for 20 h, and eventually calcined at 200 °C for 10 h.

2.3. Characterization. The synthesized PBA surface morphology was examined via an electron microscope (SEM; Japan Electro Company) connected to energy-dispersive X-ray analysis for elemental mapping (EDX) to record the main elemental composition and purity of the nanoparticles. The mean size and microstructure of the nanosheets were identified by transmission electron microscopy (TEM; Hitachi-H-7500, Japan) worked at 200 kV. A Thermo Fisher Scientific ESCALAB, USA was used for X-ray photoelectron spectroscopy (XPS) analysis. To investigate the crystal structure of the CoTCNi/HCCr complex, X-ray diffraction (XRD) (Model; Rigaku Smart Lab.) was carried out at a wavelength 1.540 Å using Cu Kα radiation over a 2θ range of 5−60°. The phase content and composition were recorded by Raman spectroscopy (Horiba Lab RAM HR Evolution). A PBA thin film was deposited on glass substrates by spin coaters (SpinNXG-P1AC). UV−vis optical absorbance was measured by a spectrophotometer (Jasco-V-570) for studying the optical properties of the thin film.

2.4. Study of the Catalytic Activity of PBA toward Reduction of 4-Nitroaniline. The reduction of 4-NA to pPDA was carried out in an aqueous medium utilizing sodium borohydride as a reducing agent and PBA as nanocatalyst. The UV−vis spectrophotometry method was utilized to track the reaction's progress. In this experiment, a quartz cuvette was filled with 2.5 mL of ultrapure water, 100 μL of an aqueous solution of 4-nitroaniline (C = 3 mM), 400 μL of an aqueous solution of $NaBH_4$ (C = 300 mM), and 50 μL of an aqueous suspension of PBA (C = 1000 μg mL^{-1}). The UV−vis spectra were recorded over the scanning range of 200−550 nm at predetermined intervals. The progress of the reaction was monitored by measuring the absorbance of 4-NA at various time intervals at 380 nm at ambient temperature. Blank experiments were additionally done by repeating the same steps but in the presence of $NaBH_4$ only without catalyst.

3. RESULTS AND DISCUSSION

3.1. Structural, Composition, and Molecular Interaction Analysis. The XRD pattern of the PBA CoTCNi/HCCr calcined at 200 °C in the air was presented in Figure 1a. The diffraction peaks at 2θ = 17.61°, 24.88°, 35.51° corresponding to the reflection planes (200), (220), (400) are well indexed to a face-centered cubic phase and matched with the standard card (JCPDS No. 82-2284, space group $Fm3m$).[29,30] As described, the pattern of broadening weak peaks with low intensity suggests poor crystal structure and small crystallite size of the nanomaterial PBA. The structure disorder is attributed to the prepared PBA's low annealing temperature or the rapid reaction rate due to the coprecipitation approach. Additionally, the presence of $Cr(CN)_6$ vacancy significantly impacts the PBA structure leading to lattice strain induce porosity production especially when the particle size of the PBA is reduced to the nanoscale dimensions.[30,31]

The atomic composition and purity of the synthesized PBA nanoparticles were recorded by EDX spectrum as described in Figure 1b. The spectrum revealed the coexistence of the main elements carbon (C), nitrogen (N), cobalt (Co), nickel (Ni), and chromium (Cr) elements without further impurities or unreacted ions.[32] Despite the prepared nanomaterial's high purity, two EDX peaks were observed at 0.525 and 1.978 keV, which were attributed to the presence of oxygen (O) and iridium (Ir) inside the host framework material. It is important to note that the spectrum of oxygen is owing to annealing the sample at 200 °C in the air whereas the iridium element is associated with coating the sample to improve its conductivity.

https://doi.org/10.1021/acsomega.2c05694
ACS Omega 2022, 7, 43139−43146

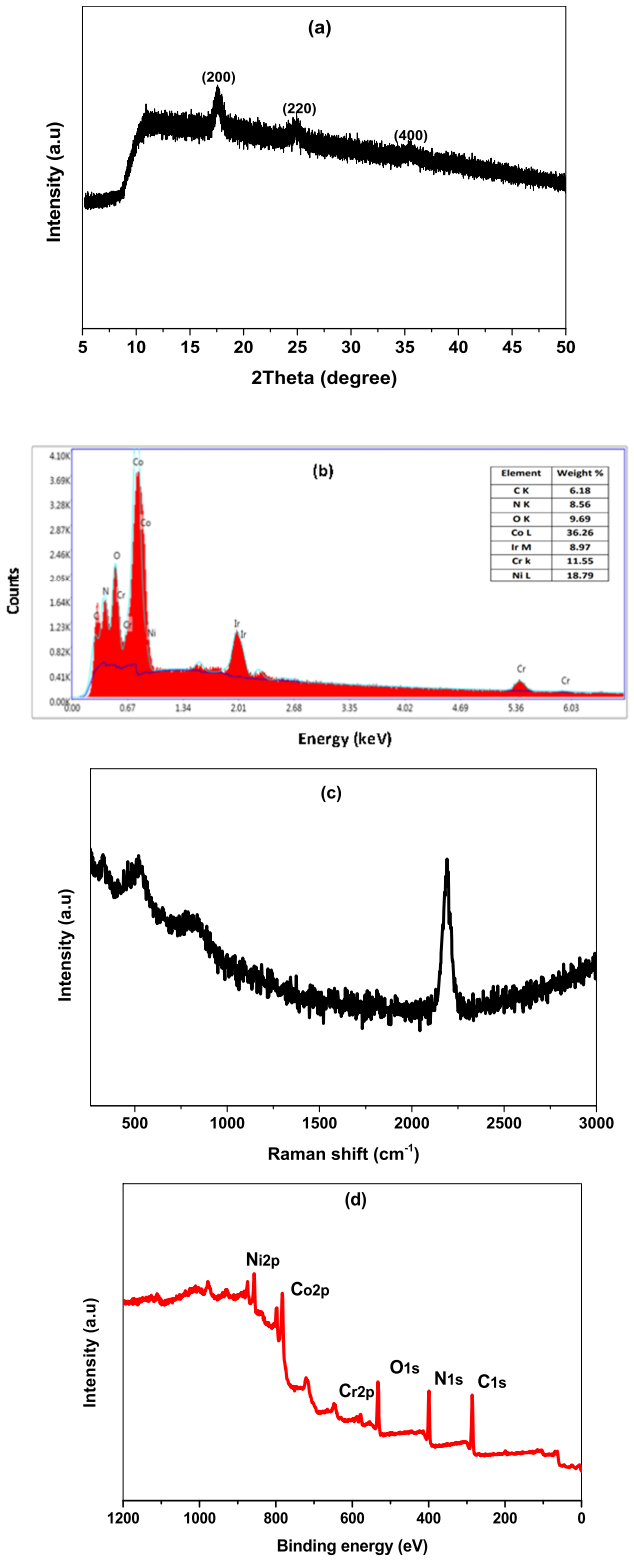

Figure 1. (a) XRD, (b) EDX, (c) Raman spectra, and (d) XPS survey for CoTCNi/HCCr nanoparticles.

The structure, phase, and molecular interaction of CoTCNi/HCCr were visualized by Raman spectroscopy through the wavenumber range from 200 to 3000 cm^{-1}. Raman spectra for the PBA show the most intense Raman peak between 2100 and 2300 cm^{-1} which is assigned to the cyanide stretching region. For the PBA precursors, potassium tetracyanonickelate (II), and potassium hexacyanochromate (III), cyanide stretching has been reported in the literature to be 2132 and 2130 cm^{-1}, respectively,[33,34] and the cyanide peak is shifted when the cyanometallate salt is coordinated with metal.[35] Figure 1c shows four vibrational modes, the main strong Raman peak located at around 2193 cm^{-1} ascribed to Ni−C≡N−Co molecular interaction. Generally, cobalt ions are octahedrally connected to the nitrogen side of the $(C{\equiv}N)^-$ anion group whereas nickel ions are connected to the carbon side of the PBA framework. Additionally, the broad weak Raman band observed at 520 cm^{-1} is attributed to the chromium−carbon Cr−C stretching vibration.[36,37] In addition, the weak band located at wavenumber 830 cm^{-1} belongs to the metal−oxygen molecular interaction, which may be owing to chromium−oxygen (Cr−O) vibration.[38] Further, because of the highly sensitive spectroscopic behavior of the cyanide group to the coordinated metals, the weak Raman modes may be associated with Cr−C≡N−O vibration. Moreover, the weak band at 320 cm^{-1} is owing to Co−O stretching. It is worth noting that the weak Raman bands is attributed to the lattice disorder or presence of defects inside the lattice which are clearly matched with the XRD pattern.[39,40]

The chemical composition of the nanomaterial surface was investigated by XPS as a sensitive technique to explain the surface compositions and chemical states of the pure PBA, and the results are displayed in Figure 1d. The XPS survey spectra reveal the presence of a characteristic peak at binding energy equal to 398.60 eV related to the nitrogen atoms where the peak for C 1s appearing at 286.98 eV confirmed the presence of the nitrile group (C≡N).[37,41] In the Ni 2p spectrum as shown in the Supporting Information (Figure S1), two nickel species could be identified in the Ni 2p XPS spectra; the Ni_{2p} XPS spectrum corresponds to Ni^{3+} located at 856.0 and 873.9 where the $Ni_{2p3/2}$ at nearly 856.06 and 873.57 eV os related to Ni^{2+}.[41,42] Furthermore, the O 1s region deconvoluted into one peak at the 533.32 eV binding energies can be assigned to the core level of oxygen in adsorbed water. Two intense peaks at the 781.93 and 796.57 eV binding energies correspond to Co $2p_{3/2}$ and Co $2p_{1/2}$ orbits appearing at a high-resolution XPS spectrum of the Co 2p region. The survey spectrum of the nanoparticles reveals the appearance of two peaks with their 3/2 branch at 576.82 and 587.58 eV, which is associated with Cr^{3+} where the peak at 578.58 eV binding energy can be correlated to the presence of Cr^{6+}.[43]

3.2. Microstructure and Morphological Analysis. The microstructure, surface morphology, and particle distribution of the PBA were identified from SEM and TEM demonstrated in Figure 2. The SEM micrograph (Figure 2a) described the particle growth in the nanosheet-like structure of high density on the surface.[44] The TEM at different magnifications shows the prepared nanomaterial of irregular ultrathin sheets with a large surface area. The mean size of the nanosheets was estimated to be around 100−200 nm.[45] As seen, some of the nanosheets were aggregated together attributed to the high surface energy and the size confinement effect.

3.3. Absorbance, Diffuse Reflection, and Energy Gap of the CoTCNi/HCCr Thin Film. The UV−vis optical absorbance of CoTCNi/HCCr coated on a glass substrate thin film was measured through the UV−vis spectrum as illustrated in Figure 3a. The spectrum has a strong absorption band at 282 nm attributed to the interaction of incident photon energy and the particles of PBA.[46,47] Figure 3b demonstrates the diffuse reflection of CoTCNi/HCCr as a

https://doi.org/10.1021/acsomega.2c05694
ACS Omega 2022, 7, 43139−43146

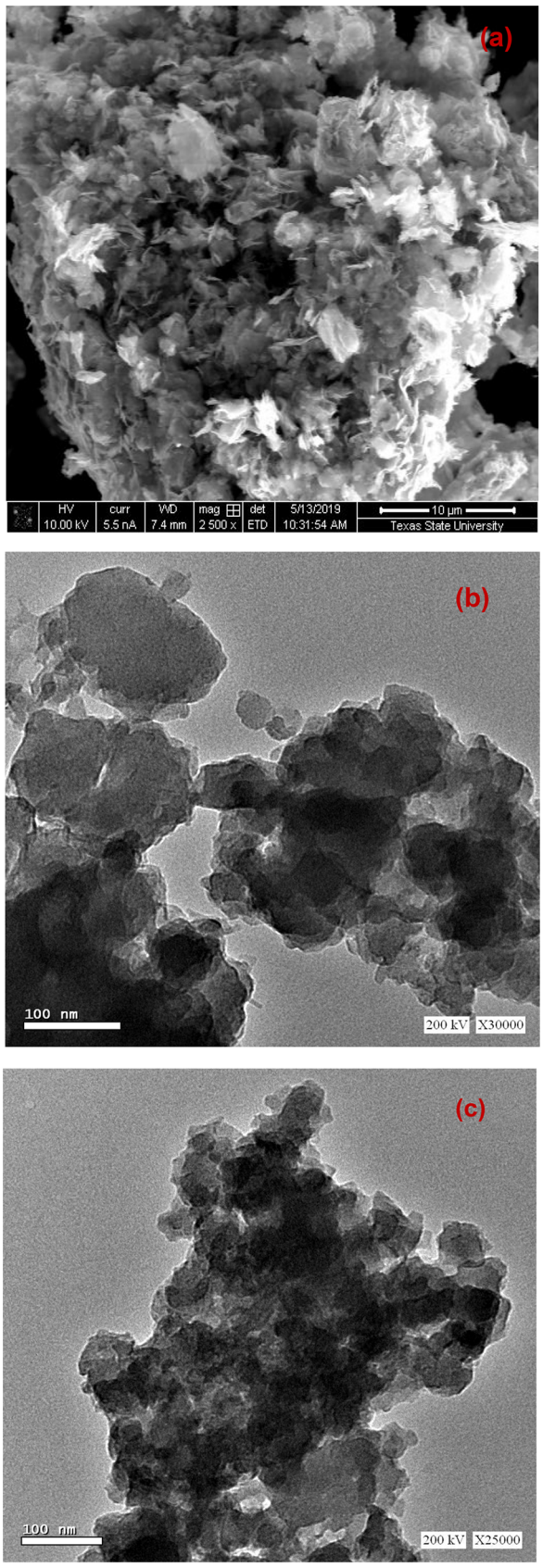

Figure 2. (a) SEM and (b, c) TEM micrographs of PBA CoTCNi/HCCr.

function of applied wavelength. The film exhibited peaks and valleys inside the UV region attributed to the strong photon–

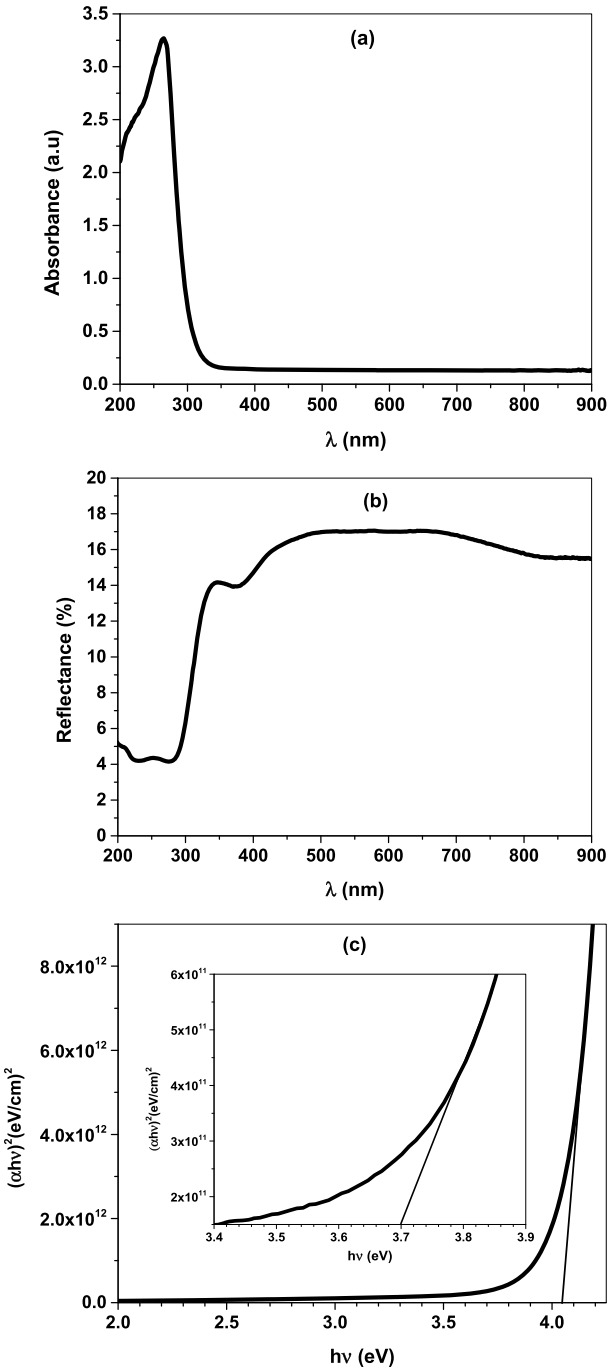

Figure 3. (a) Absorbance spectrum, (b) reflectance spectrum, and (c) energy gap plot of the PBA thin film.

electron interaction and scattering of the incident photon energy on the film surface at different angles.[47,48] The band gap (E_g) is an important optical parameter that defines the electronic characteristics and type of electron transition of the nanomaterial. E_g of the fabricated thin film was determined from Tauc's formula given by eq 1[47]

$$\alpha = \frac{A}{h\nu}(h\nu - E_g)^n \quad (1)$$

where $h\nu$ is the incident optical energy, A is the optical absorbance, and α is the optical absorption coefficient expressed as eq 2[47]

https://doi.org/10.1021/acsomega.2c05694
ACS Omega 2022, 7, 43139−43146

$$\alpha = \frac{2.303A}{t} \quad (2)$$

where t is the thickness of the film was 300 nm. The E_g was evaluated by extending the straight line part of the $(\alpha h\nu)^2$ curve on the Y-axis to the energy on the X-axis at $(\alpha h\nu)^2 = 0$ (Figure 3c) indicating a wide band gap of allowed direct transitions.[49] The optical behavior indicates the direct transition of electrons through an optical band gap in the range 3.70−4.05 eV. The photon energy greater than the band gap means that more electrons transfer from to the conduction band leading to an increase in the free charge carriers.[50] Further, the wide optical band gap materials have peculiar properties in the biomedical field and chemical sensor devices that can operate at much higher applied frequencies and high temperatures. Also, it can easily absorb or emit ultraviolet light with high performance.

3.4. Catalytic Reduction of 4-Nitroaniline Using PBA.

Nitroanilines are hazardous environmental contaminants which are released by several industries. Therefore, it is necessary to transform them into less harmful compounds, like *p*-phenylenediamine (*p*-PDA). The catalytic activity of PBA was investigated by reducing 4-NA to utilize $NaBH_4$ as a reducing agent in aqueous media as presented in Figure 4. The

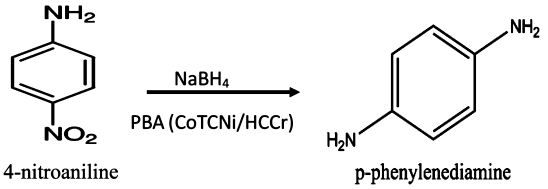

Figure 4. Reduction of 4-nitroaniline to *p*-phenylendiamine by $NaBH_4$ using PBA (CoTCNi/HCCr) as nanocatalyst.

reduction process was monitored by UV−vis spectrophotometry by scanning at definite intervals.[51] It was found that the peak of 4-NA gradually decreased at 380 nm with time and completely vanished after 270 s as shown in Figure 5. Furthermore, a new peak corresponding to *p*-phenylenediamine (*p*-PDA) was simultaneously observed at 240 nm.[52] The

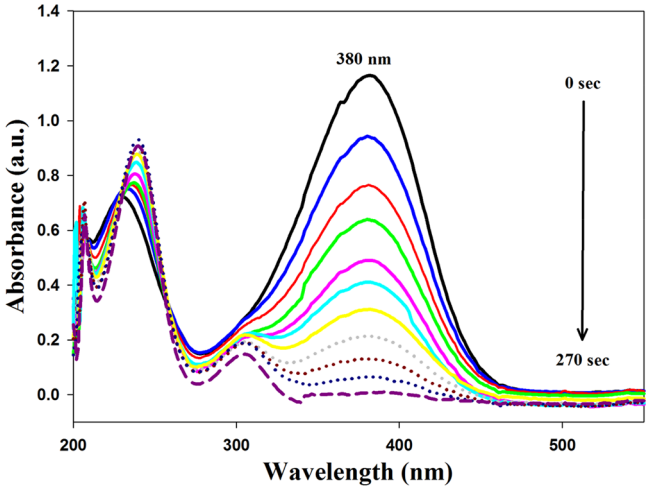

Figure 5. UV−vis spectra for the reduction of 4-nitroaniline compound by PBA (CoTCNi/HCCr) at various time intervals.

reaction mixture solution changed from bright yellow to colorless after the reaction was finished.

Additionally, reduction of 4-NA utilizing $NaBH_4$ was tested in the absence of the nanocatalyst, Figure 6. It was found that a

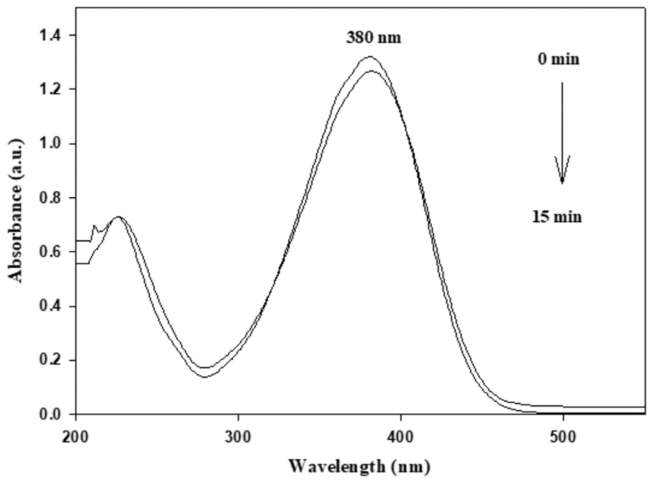

Figure 6. UV−visible spectra for the reduction of 4-nitroaniline compound without using a catalyst.

very small amount of 4-NA was reduced to *p*-PDA in 15 min due to the slowness of the reduction reaction. Even though the reduction of 4-NA by $NaBH_4$ is thermodynamically favorable, the substantial energy barrier between the electron donor and electron acceptor species makes it kinetically unfavorable.[53] Consequently, PBA plays a crucial role in the transport of electrons from BH_4^{-1} to 4-NA by overcoming the energy barrier and, hence, quickens the reduction process.

A pseudo-first-order kinetic model was utilized to assess the rate constant for reduction of 4-NA because the $NaBH_4$ concentration was present in excessive amount relative to 4-NA concentration. As a result, it was assumed that the rate of reaction was solely reliant on the concentration of 4-NA. The utilized pseudo-first-order kinetic equation is described as $\ln(C_t/C_o) = -kt$.[54] However, the ratio of C_t/C_o can be computed in terms of absorbance ratio A_t/A_o since it is equal at 380 nm. A plot of $\ln(A_t/A_o)$ against time for the reduction of 4-NA utilizing PBA (CoTCNi/HCCr) as a catalyst is illustrated in Figure 7. It was observed that the value of $\ln(A_t/A_o)$ decreased with time due to a decrease in 4-NA concentration, and k was determined from the slope of the

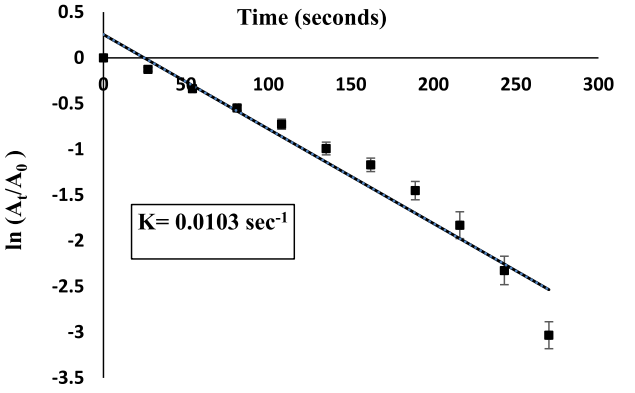

Figure 7. Kinetics plot of $\ln(A_t/A_o)$ against time for reduction of 4-nitroaniline using PBA (CoTCNi/HCCr) as nanocatalyst.

https://doi.org/10.1021/acsomega.2c05694
ACS Omega 2022, 7, 43139−43146

illustrated plot which was found to be 0.0103 s^{-1}. Moreover, a comparison of the catalytic activity of the proposed PBA (CoTCNi/HCCr) was done with the other catalysts reported in the literature, and the results are illustrated in Table 1. It is clear that PBA (CoTCNi/HCCr) has excellent catalytic activity in the reduction of 4-nitroaniline when compared to the other catalysts in the literature.

Table 1. Comparison of the Catalytic Efficiency of the Suggested Prussian Blue Analogue (PBA) (CoTCNi/HCCr) with the Other Reported Catalysts for Reduction of 4-Nitroaniline

Catalyst	Total Reduction Time	K	Ref
RGO−Ni NPs	190 min	1.296×10^{-2} min^{-1}	55
Cu−CuO nanocomposite	8 min	0.305 min^{-1}	56
$CuNi/Co_3O_4$	21 min	1.71×10^{-3} min^{-1}	57
(PbA) (CoTCNi/HCCr)	270 s	0.0103 s^{-1}	our work

3.5. Effect of Catalyst Dose and pH of Medium on Catalytic Activity of PBA (CoTCNi/HCCr) Nanocatalyst. During optimization, the effect of the catalyst dosage was initially investigated. It has been demonstrated that the reaction was very fast upon increasing the catalyst dosage to 100 μg so the optimum utilized catalyst dosage was 50 μg as a lower dose exhibited longer reduction time. Consequently, the chosen catalyst dosage was 50 μg at which the total reduction time occurred within 270 s with calculated rate constants (k) equals 0.0103 s^{-1}.

Moreover, the influence of pH on the catalytic reduction of 4-NA by $NaBH_4$ was examined under three various conditions (acidic; pH 5, neutral; 7 and basic; pH 9). The reduction rate was investigated while maintaining the nanocatalyst concentration and other factors constant. The optimum catalytic reduction of 4-NA was found to be under neutral conditions (pH 7). However, as the pH declined, the rate slowed down and a very small amount of 4-NA (8%) was reduced in 14 min probably due to the fact that $NaBH_4$ hydrolyzes quickly in acidic medium. Nevertheless, the reduction rate was moderate in the alkaline medium as the total reduction time occurred within 330 s, which is slightly higher than the neutral pH.

3.6. Reusability of the Proposed PBA (CoTCNi/HCCr) Nanocatalyst. The reusability of the suggested nanoparticles PBA (CoTCNi/HCCr) was tested to evaluate their practical catalytic applications. This was done by repeating the reduction process using the same catalyst. A new batch of 4-NA was added to the reaction mixture after finishing one catalytic reduction cycle without catalyst regeneration. It was found that the PBA (CoTCNi/HCCr) catalyst exhibited nearly the same catalytic performance after five successive reaction cycles. The total reduction time slightly increased. Nevertheless, the PBA (CoTCNi/HCCr) was still able to completely and quickly reduce 4-NA to p-PDA even in the absence of regeneration, demonstrating good catalytic activity and high stability of these PBAs in this process. Moreover, the reusability experiments of the proposed nanoparticles demonstrated that approximately 95% of 4-NA was reduced even after the fifth cycle, which indicates that they have good performance stability (Figure 8).

4. CONCLUSION

In this work, novel PBA nanoparticles were successfully synthesized via chemical coprecipitation to be used as an efficient nanocatalyst for the reduction of nitroanilines. PBA (CoTCNi/HCCr) was characterized by various techniques such as XRD, EDX, XPS, Raman spectroscopy, SEM, and TEM. The PBA nanoparticles are highly promising candidates for fast reduction of the environmentally hazardous 4-NA into the respective harmless p-PDA. The total reduction time of 4-NA occurred within 270 s with calculated rate constants (k) equal to 0.0103 s^{-1}. Eventually, the proposed PBA nanoparticles could be used as potential nanocatalysts for the reduction of other hazardous nitroaromatics and pave the way toward future applications in biomedical and catalytic fields.

■ ASSOCIATED CONTENT

Supporting Information

The Supporting Information is available free of charge at https://pubs.acs.org/doi/10.1021/acsomega.2c05694.

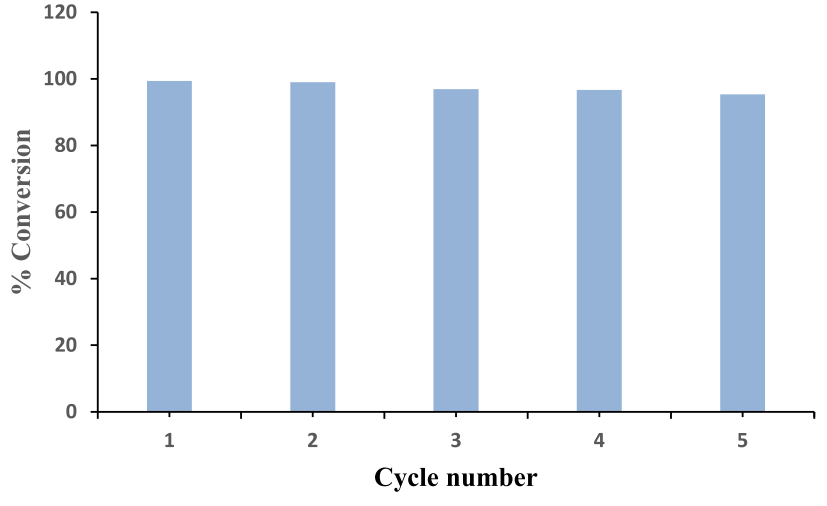

Figure 8. Conversion rate of 4-NA using PBA (CoTCNi/HCCr) as nanocatalyst after five different cycles.

https://doi.org/10.1021/acsomega.2c05694
ACS Omega 2022, 7, 43139−43146

Data of high-resolution XPS spectra of CoTCNi/HCCr including C 1s, N 1s, Co 2p, Ni 2p, Cr 2p, and O 1s (PDF)

AUTHOR INFORMATION

Corresponding Authors

Amr M. Mahmoud − *Analytical Chemistry Department, Faculty of Pharmacy, Cairo University, 11562 Cairo, Egypt*; orcid.org/0000-0002-7804-6442; Email: amr.bekhet@pharma.cu.edu.eg

Ahmed M. Abdel-Raoof − *Pharmaceutical Analytical Chemistry Department, Faculty of Pharmacy (Boys), Al-Azhar University, 11751 Nasr City, Cairo, Egypt*; Email: ahmedmeetyazeed79@azhar.edu.eg

Authors

Dina A. El Mously − *Analytical Chemistry Department, Faculty of Pharmacy, Cairo University, 11562 Cairo, Egypt*

Elsayed Elgazzar − *Department of Physics, Faculty of Science, Suez Canal University, 41522 Ismailia, Egypt*

Complete contact information is available at: https://pubs.acs.org/10.1021/acsomega.2c05694

Notes

The authors declare no competing financial interest.

ACKNOWLEDGMENTS

The authors would like to thank both the Analytical Chemistry Department, Faculty of Pharmacy, Cairo University and Department of Physics, Faculty of Science, Suez Canal University for providing the chemicals and facilities to accomplish this work.

REFERENCES

(1) Farooqi, Z. H.; Naseem, K.; Begum, R.; Ijaz, A. Catalytic reduction of 2-nitroaniline in aqueous medium using silver nanoparticles functionalized polymer microgels. *J. Inorg. Organomet. Polym. Mater.* **2015**, *25* (6), 1554−1568.

(2) Farooqi, Z. H.; Naseem, K.; Ijaz, A.; Begum, R. Engineering of silver nanoparticle fabricated poly (N-isopropylacrylamide-co-acrylic acid) microgels for rapid catalytic reduction of nitrobenzene. *J. Polym. Eng.* **2016**, *36* (1), 87−96.

(3) Naseem, K.; Begum, R.; Farooqi, Z. H. Catalytic reduction of 2-nitroaniline: a review. *Environ. Sci. Pollut. Res.* **2017**, *24* (7), 6446−6460.

(4) Dong, Z.; Le, X.; Li, X.; Zhang, W.; Dong, C.; Ma, J. Silver nanoparticles immobilized on fibrous nano-silica as highly efficient and recyclable heterogeneous catalyst for reduction of 4-nitrophenol and 2-nitroaniline. *Appl. Catal., B* **2014**, *158*, 129−135.

(5) Mei, X.; Ding, Y.; Wang, Y.; Yang, Y.; Xu, L.; Wang, Y.; Shen, W.; Zhang, Z.; Ma, M.; Guo, Z. A novel membrane-aerated biofilter for the enhanced treatment of nitroaniline wastewater: Nitroaniline biodegradation performance and its influencing factors. *Bioresour. Technol.* **2020**, *307*, 123241.

(6) Begum, R.; Naseem, K.; Ahmed, E.; Sharif, A.; Farooqi, Z. H. Simultaneous catalytic reduction of nitroarenes using silver nanoparticles fabricated in poly (N-isopropylacrylamide-acrylic acid-acrylamide) microgels. *Colloids Surf., A* **2016**, *511*, 17−26.

(7) Malakootian, M.; Khatami, M.; Mahdizadeh, H.; Nasiri, A.; Amiri Gharaghani, M. A study on the photocatalytic degradation of p-Nitroaniline on glass plates by Thermo-Immobilized ZnO nanoparticle. *Inorg. Nano-Met. Chem.* **2020**, *50* (3), 124−135.

(8) Gangemi, C. M. A.; Iudici, M.; Spitaleri, L.; Randazzo, R.; Gaeta, M.; D'Urso, A.; Gulino, A.; Purrello, R.; Fragalà, M. E. Polyethersulfone mats functionalized with porphyrin for removal of para-nitroaniline from aqueous solution. *Molecules* **2019**, *24* (18), 3344.

(9) Yamuna, A.; Jiang, T.-Y.; Chen, S.-M. Preparation of K+ intercalated MnO2-rGO composite for the electrochemical detection of nitroaniline in industrial wastewater. *J. Hazard. Mater.* **2021**, *411*, 125054.

(10) El-Masry, M. M.; El-Shahat, M.; Ramadan, R.; Abdelhameed, R. M. Selective photocatalytic reduction of nitroarenes into amines based on cobalt/copper ferrite and cobalt-doped copper ferrite nano-photocatalyst. *J. Mater. Sci.: Mater. Electron.* **2021**, *32* (13), 18408−18424.

(11) Liu, H.-Y.; Niu, C.-G.; Guo, H.; Liang, C.; Huang, D.-W.; Zhang, L.; Yang, Y.-Y.; Li, L. In suit constructing 2D/1D MgIn2S4/CdS heterojunction system with enhanced photocatalytic activity towards treatment of wastewater and H2 production. *J. Colloid Interface Sci.* **2020**, *576*, 264−279.

(12) Laghrib, F.; Aghris, S.; Ajermoun, N.; Hrioua, A.; Bakasse, M.; Lahrich, S.; El Mhammedi, M. A. Recent progress in controlling the synthesis and assembly of nanostructures: Application for electrochemical determination of p-nitroaniline in water. *Talanta* **2020**, *219*, 121234.

(13) Mal, D.; Alveroglu, E.; Balouch, A.; Jagirani, M. S.; Abdullah; Kumar, S. Highly efficient and selective heterogeneous catalytic reduction of 2-nitroaniline by cerium oxide nanocatalyst under microwave irradiation. *Environmental Technology* **2022**, *43*, 3631.

(14) Wang, R.-L.; Li, D.-P.; Wang, L.-J.; Zhang, X.; Zhou, Z.-Y.; Mu, J.-L.; Su, Z.-M. The preparation of new covalent organic framework embedded with silver nanoparticles and its applications in degradation of organic pollutants from waste water. *Dalton Trans.* **2019**, *48* (3), 1051−1059.

(15) Wang, R.; Cai, C.; Wang, D.; Liu, Z.; Gao, L.; Jiao, T. Self-assembled Au/Fe3O4 nanoparticle-loaded phytic acid-graphene oxide composite foam with highly efficient catalytic performance for p-nitrophenol and o-nitroaniline organic pollutants. *Colloids Surf., A* **2021**, *617*, 126368.

(16) Elsayed, G. M.; El Mously, D. A.; Mostafa, N. M.; Hassan, N. Y.; Mahmoud, A. M. Neostigmine potentiometric sensors based on microfabricated copper electrodes using Poly (3-octylthiophene) as an ion-to-electron transducer layer. *J. Electrochem. Soc.* **2020**, *167* (13), 137506.

(17) Atta, M. Y.; Hegazy, M. A.; Mahmoud, A. M.; Ghoniem, N. S. Electrochemical Sensor for Meropenem Therapeutic Monitoring in Human Plasma Based on Carbon Nanotubes Modified Basal Pyrolytic Graphite Electrode. *J. Electrochem. Soc.* **2022**, *169* (9), No. 097504.

(18) Ghorbani-Vaghei, R.; Veisi, H.; Aliani, M. H.; Mohammadi, P.; Karmakar, B. Alginate modified magnetic nanoparticles to immobilization of gold nanoparticles as an efficient magnetic nanocatalyst for reduction of 4-nitrophenol in water. *J. Mol. Liq.* **2021**, *327*, 114868.

(19) Lahtinen, E.; Kukkonen, E.; Kinnunen, V.; Lahtinen, M.; Kinnunen, K.; Suvanto, S.; Väisänen, A.; Haukka, M. Gold Nanoparticles on 3D-printed filters: From waste to catalysts. *ACS omega* **2019**, *4* (16), 16891−16898.

(20) Albukhari, S. M.; Ismail, M.; Akhtar, K.; Danish, E. Y. Catalytic reduction of nitrophenols and dyes using silver nanoparticles cellulose polymer paper for the resolution of waste water treatment challenges. *Colloids Surf., A* **2019**, *577*, 548−561.

(21) Antony, R.; Marimuthu, R.; Murugavel, R. Bimetallic nanoparticles anchored on core−shell support as an easily recoverable and reusable catalytic system for efficient nitroarene reduction. *ACS omega* **2019**, *4* (5), 9241−9250.

(22) Xie, B.; Sun, B.; Gao, T.; Ma, Y.; Yin, G.; Zuo, P. Recent progress of Prussian blue analogues as cathode materials for nonaqueous sodium-ion batteries. *Coord. Chem. Rev.* **2022**, *460*, 214478.

(23) Cao, L.-M.; Lu, D.; Zhong, D.-C.; Lu, T.-B. Prussian blue analogues and their derived nanomaterials for electrocatalytic water splitting. *Coord. Chem. Rev.* **2020**, *407*, 213156.

(24) Zhao, Y.; Liang, B.; Wei, X.; Li, K.; Lv, C.; Zhao, Y. A core-shell heterostructured CuFe NiFe Prussian blue analogue as a novel

electrode material for high-capacity and stable capacitive deionization. *J. Mater. Chem. A* **2019**, *7* (17), 10464−10474.
(25) Guari, Y.; Larionova, J.*Prussian blue-type nanoparticles and nanocomposites: synthesis, devices, and applications*; CRC Press, 2019.
(26) Guari, Y.; Cahu, M. l.; Félix, G.; Sene, S.; Long, J. r. m.; Chopineau, J. l.; Devoisselle, J.-M.; Larionova, J. Nanoheterostructures based on nanosized Prussian blue and its Analogues: Design, properties and applications. *Coord. Chem. Rev.* **2022**, *461*, 214497.
(27) Liang, J.; Li, C. H.; Talham, D. R. Growth mechanisms of mesoscale Prussian blue analogue particles in modifier-free synthesis. *Cryst. Growth Des.* **2020**, *20* (4), 2713−2720.
(28) Guo, L.; Mo, R.; Shi, W.; Huang, Y.; Leong, Z. Y.; Ding, M.; Chen, F.; Yang, H. Y. A Prussian blue anode for high performance electrochemical deionization promoted by the faradaic mechanism. *Nanoscale* **2017**, *9* (35), 13305−13312.
(29) Elgazzar, E.; Abdel-Raoof, A. M.; El-Attar, A.-A. M.; Ashmawy, A. M.; Abdulla, S. A. An extremely sensitive carbon paste electrode modified with Prussian blue analogue (PbA CPE) for the electrochemical determination of Tetramisole HCl anthelmintic drug as a food contaminant in beef cuts and infant formula milk powder. *Microchem. J.* **2022**, *178*, 107413.
(30) Nakotte, H.; Shrestha, M.; Adak, S.; Boergert, M.; Zapf, V. S.; Harrison, N.; King, G.; Daemen, L. Magnetic properties of some transition-metal Prussian Blue Analogs with composition M3 [M′(C, N) 6] 2· xH2O. *J. Sci.: Adv. Mater. Devices* **2016**, *1* (2), 113−120.
(31) Xie, B.; Sun, B.; Gao, T.; Ma, Y.; Yin, G.; Zuo, P. Recent progress of Prussian blue analogues as cathode materials for nonaqueous sodium-ion batteries. *Coord. Chem. Rev.* **2022**, *460*, 214478.
(32) Elgazzar, E. Prussian blue analogue cobalt tetracyanonickelate hexacyanochromate decorated by CNTs: structural, morphological, optical characterization. *Mater. Res. Express* **2020**, *7* (7), No. 075004.
(33) Waage Jensen, P. Solution and single crystal raman spectra of potassium hexacyanochromate (III). *J. Mol. Struct.* **1973**, *17* (2), 377−388.
(34) McCullough, R.; Jones, L.; Crosby, G. An analysis of the vibrational spectrum of the tetracyanonickelate (II) ion in a crystal lattice. *Spectrochim. Acta* **1960**, *16* (8), 929−944.
(35) Maynard, B. A.; Lynn, K. S.; Sykora, R. E.; Gorden, A. E. Emission, Raman spectroscopy, and structural characterization of actinide tetracyanometallates. *Inorg. Chem.* **2013**, *52* (9), 4880−4889.
(36) Darweish, E.; Abdel-Raoof, A. M.; Marzouk, H. M.; Ashmawy, A. M.; Fayez, Y. M.; Eissa, M. S. Innovative pH-dependent approach for electrochemical determination of a triple eradication therapy targeting H. Pylori infection in pharmaceutical formulation and human plasma sample: Modified electrode with Prussian blue analogue decorated multi-walled carbon nanotubes (PbA@ MWCNT). *Microchem. J.* **2022**, *181*, 107784.
(37) Shen, Y.-M.; Gao, M.-Y.; Chen, X.; Shen, A.-G.; Hu, J.-M. Fine synthesis of Prussian-blue analogue coated gold nanoparticles (Au PBA NPs) for sorting specific cancer cell subtypes. *Spectrochim. Acta, Part A* **2021**, *252*, 119566.
(38) Vaskova, H.Raman microscopic detection of chromium compounds. In *MATEC Web of Conferences*; EDP Sciences, 2016; Vol. *76*, p 05012.
(39) Kürkçüoğlu, G. S.; Yeşilel, O. Z.; Sayın, E.; Enönlü, E.; Şahin, O. Synthesis and structural analysis of heteronuclear hexacyanochromate (III) complex with tris (2-aminoethyl) amine),[Cd (tren)-(Htren)][Cr (CN) 6]· 2H2O. *J. Mol. Struct.* **2020**, *1219*, 128462.
(40) Safizadeh, F.; Ghasemian-Langeroudi, E.; Gagnon, C.; Larachi, F. J. S. S. Technology. Detection and identification of cobalt cyanide complexes using capillary electrophoresis. *Sep. Sci. Technol.* **2014**, *49* (5), 691−701.
(41) Huang, M.; Wang, Y.; Song, M.; Chen, F. Bimetallic CuCo Prussian blue analogue nanocubes induced chemiluminescence of luminol under alkaline solution for uric acid detection in human serum. *Microchem. J.* **2022**, *181*, 107667.
(42) Gong, A.; Zhao, Y.; He, M.; Liang, B.; Li, K. High-performance desalination of three-dimensional nitrogen-doped carbon framework reinforced Prussian blue in capacitive deionization. *Desalination* **2021**, *505*, 114997.
(43) Cortazar-Martinez, O.; Torres-Ochoa, J.-A.; Raboño Borbolla, J.-G.; Herrera-Gomez, A. Oxidation mechanism of metallic chromium at room temperature. *Appl. Surf. Sci.* **2021**, *542*, 148636.
(44) Yang, Z.; Niu, H.; Yu, F.; Xie, X.; Qian, K.; Bian, K.; Xiang, M.; Dong, S. Manganese and cobalt bimetallic-doped Prussian blue analogs as a bifunctional electrocatalyst for zinc-air batteries. *J. Colloid Interface Sci.* **2022**, *628*, 588.
(45) Huang, H.; Xue, Q.; Zhang, Y.; Chen, Y. Two-dimensional cobalt prussian blue nanosheets: Template-directed synthesis and electrocatalytic oxygen evolution property. *Electrochim. Acta* **2020**, *333*, 135544.
(46) Mamontova, E.; Rodríguez−Castillo, M.; Oliviero, E.; Guari, Y.; Larionova, J.; Monge, M.; Long, J. r. m. Designing heterostructured core satellite Prussian Blue Analogue Au-Ag nanoparticles: Effect on the magnetic properties and catalytic activity. *Inorg. Chem. Front.* **2021**, *8* (9), 2248−2260.
(47) Elgazzar, E. Improvement the efficacy of Al/CuPc/n-Si/Al Schottky diode based on strong light absorption and high photocarriers response. *Mater. Res. Express* **2020**, *7* (9), No. 095102.
(48) Parra, M. R.; Haque, F. Z. Aqueous chemical route synthesis and the effect of calcination temperature on the structural and optical properties of ZnO nanoparticles. *J. Mater. Res. Technol.* **2014**, *3* (4), 363−369.
(49) Rani, M.; Shanker, U. Metal hexacyanoferrates nanoparticles mediated degradation of carcinogenic aromatic amines. *Environ. Nanotechnol., Monit. Manage.* **2018**, *10*, 36−50.
(50) Bass, M.; DeCusatis, C.; Enoch, J.; Lakshminarayanan, V.; Li, G.; MacDonald, C.; Mahajan, V.; Van Stryland, E.Handbook of Optics, Volume IV: Optical Properties of Materials*Nonlinear Opt., Quantum Opt.*; McGraw Hill, 2009; Vol. *4*.
(51) El Mously, D. A.; Mostafa, N. M.; Hassan, N. Y.; El-Sayed, G. M. Different Approaches in Manipulating Ratio Spectra for Analyzing Amlodipine Besylate and Irbesartan Combination. *J. AOAC Int.* **2022**, *105* (5), 1219−1227.
(52) Zhou, Q.; Qian, G.; Li, Y.; Zhao, G.; Chao, Y.; Zheng, J. Two-dimensional assembly of silver nanoparticles for catalytic reduction of 4-nitroaniline. *Thin Solid Films* **2008**, *516* (6), 953−956.
(53) Farooqi, Z. H.; Khan, S. R.; Hussain, T.; Begum, R.; Ejaz, K.; Majeed, S.; Ajmal, M.; Kanwal, F.; Siddiq, M. Effect of crosslinker feed content on catalaytic activity of silver nanoparticles fabricated in multiresponsive microgels. *Korean J. Chem. Eng.* **2014**, *31* (9), 1674−1680.
(54) El-Sayed, G. M.; El Mously, D. A.; Mostafa, N. M.; Hassan, N. Y.; Mahmoud, A. M. Design of Copper Microfabricated Potentiometric Sensor for inline Monitoring of Neostigmine Degradation Kinetics. *Electroanalysis* **2021**, *33* (5), 1215−1224.
(55) Das, P.; Ghosh, S. Heterogeneous catalytic reduction of 4-nitroaniline by RGO-Ni nanocomposite for water resource management. *J. Mater. Sci.: Mater. Electron.* **2019**, *30* (22), 19731−19737.
(56) Revathi, K.; Palantavida, S.; Vijayan, B. K. Effective Reduction of p-Nitroaniline to p-Phenylenediamine Using Cu-CuO Nanocomposite. *Mater. Today: Proc.* **2019**, *9*, 633−638.
(57) Deka, P.; Choudhury, R.; Deka, R. C.; Bharali, P. Influence of Ni on enhanced catalytic activity of Cu/Co 3 O 4 towards reduction of nitroaromatic compounds: studies on the reduction kinetics. *RSC Adv.* **2016**, *6* (75), 71517−71528.

https://doi.org/10.1021/acsomega.2c05694
ACS Omega 2022, 7, 43139−43146